

# Maximizing Entropy by Minimizing Area: Towards a New Principle of Self-Organization

P. Ziherl\* and Randall D. Kamien

*Department of Physics and Astronomy, University of Pennsylvania, Philadelphia, PA 19104-6396*

(October 25, 2018)

We propose a heuristic explanation for the numerous non-close-packed crystal structures observed in various colloidal systems. By developing an analogy between soap froths and the soft coronas of fuzzy colloids, we provide a geometrical interpretation of the free energy of soft spheres. Within this picture, we show that the close-packing rule associated with hard-core interaction and positional entropy of particles is frustrated by a minimum-area principle associated with the soft tail and internal entropy of the soft coronas. We also discuss these ideas in terms of crystal architecture and pair distribution functions and analyze the phase diagram of a model hard-sphere-square-shoulder system within the cellular theory. We find that the A15 lattice, known to be area minimizing, is favored for a reasonable range of model parameters and so it is among the possible equilibrium states for a variety of colloidal systems. We also show that in the case of short-range convex potentials the A15 and other non-close-packed lattices coexist over a broad ranges of densities, which could make their identification difficult.

PACS numbers: 61.50.Ah, 82.70.-y

## I. INTRODUCTION

Colloids are all around us. From milk to microreactors, from pie filling to paint, and from suspensions to sieves, colloidal materials are important in a variety of products and technologies and are the basis for a new class of functional materials. The advent of applications based on engineered crystalline materials, such as photonic bandgap materials,<sup>1,2</sup> has put even greater focus on colloids. Both the size of colloidal particles and the interparticle interaction are tunable, which provides the basis for the manufacture of ordered structures with desired lattice spacings and space groups as well as mechanical, thermal, and electrical properties.

Over the years, considerable amounts of experimental crystallographic data have been collected for various colloidal systems.<sup>3</sup> While the tabulation of the relationship between the interparticle interaction and the symmetry of the crystal lattice is undoubtedly valuable, it is desirable, if not necessary, that the synthesis of colloidal crystals with specific space group be based on analytic rather than empirical insight into the mechanisms of self-assembly. In principle this should be possible because the interaction between the particles is much simpler than in atomic or molecular crystals: colloidal particles are made of hundreds or thousands of atoms, and the effective interaction between the particles is less specific and thus much simpler than interatomic interactions. Thus the interaction between colloidal particles is chiefly determined by their mechanical as opposed to chemical structure. Here we will address those colloidal particles that are characterized by a relatively dense core and a fluffy corona. In this case, the interparticle potential may be approximated fairly well by the simple hard-core repulsion dressed with a repulsive short-range interaction of finite strength.

Present theoretical understanding of the phase behavior and stability of the various colloidal systems is quite impressive, especially in the case of charged colloidal suspensions interacting via screened Coulomb potentials.<sup>4-7</sup> It is now well established both by analytical approaches<sup>4,7</sup> and by simulations<sup>5</sup> that the solid part of the phase diagram of charged colloids includes face-centered cubic (FCC) and body-centered cubic (BCC) lattices. In the case of a convex interparticle potential – its simplest variant being the square shoulder interaction<sup>8</sup> – the phase diagram is even more complex and includes the dense and the loose FCC and BCC lattices.<sup>9</sup> More elaborate soft potentials such as the interaction between star polymers lead to body-centered orthorhombic (BCO) and diamond lattices in addition to FCC and BCC lattices.<sup>10</sup>

While extremely important, these theories do not provide a robust explanation of the stability of colloidal crystals, and the aim of this study is to look at the problem from a more geometrical point of view and to capture the statistical mechanics of colloids in a new self-organization principle. One such principle is the maximum packing fraction rule, which states that pure excluded-volume interactions favor an expanded close-packed structure, thereby maximizing the configurational entropy. In the case of monodisperse hard spheres, such an arrangement corresponds to the FCC lattice.<sup>11,12</sup> However, many soft-sphere systems form non-close-packed lattices, including the BCC, BCO, and diamond lattices as well as the A15 lattice<sup>13</sup> observed in crystals of self-assembled micelles of some dendritic polymers.<sup>14</sup> Can we understand the existence of this rather loosely packed structure? Is there another simple geometrical principle that describes the self-organization of soft spheres and is analogous but opposing to the maximum packing fraction rule? We pursue this question using an idealized model and find an anal-

ogy between the soft-sphere crystals and dry soap froths, the latter being described by Kelvin’s problem of finding the minimal-area regular partition of space into cells of equal volume. Within this framework, we propose a new principle of area-minimization that can favor these loosely packed lattices of soft spheres.<sup>15</sup>

Having proposed our semiquantitative and intuitive explanation for the behavior of soft-sphere colloids, we have checked our predictions within a more rigorous statistical-mechanical model to see whether the theoretically calculated phase diagram includes some of these loose-packed structures – the A15 lattice in particular. In previous theoretical studies this structure was not considered as a trial state of a repulsive colloidal system, and the solid part of the phase diagram was shared virtually exclusively by FCC and BCC phases.<sup>4,5,7</sup> We scan the phase diagram for the case of square-shoulder soft potential, the focus of other studies, and determine the range of widths of the soft potential where the A15 lattice is the colloidal ground state.

The paper is organized as follows: in Section II, we describe our model of colloidal self-organization and establish the analogy between these systems and soap froth. We digress to describe the Kelvin problem and its conjectured solution. We show that this analogy leads to a second global principle of self-assembly – the primary one being the principle of maximum packing entropy – and that the two mechanisms give rise to frustration. We apply these ideas to a dendrimer compound (which crystallizes into the A15 lattice) as well as to other systems. In Section III we reexamine the phase diagram of the hard-core–square-shoulder interaction, which captures many features of real colloidal systems. We analyze it within the cellular free volume approximation using a numerical model whose main advantage is that the colloidal interaction is treated nonperturbatively. Section IV concludes the paper.

## II. COLLOIDAL SYSTEMS AS AREA-MINIMIZING STRUCTURES

Recently, dendrimers composed of a poly(benzyl ether) core segments decorated with dodecyl chains<sup>16</sup> were synthesized with the intention of producing a molecule with a conical, fan-shaped architecture.<sup>14</sup> Since it is known that many dendrimers spontaneously self-assemble into supramolecular clusters, the underlying rationale was motivated by the possibility of creating spherical micellar-like objects a few nanometers in diameter. These dendrimers do indeed form spheres which, in turn, form a crystal lattice with the  $Pm\bar{3}n$  space group, also known as the A15,  $Q^{223}$ , and  $\beta$ -Tungsten lattice. This lattice belongs to the cubic system, and its unit cell includes 8 sites which can be divided into 3 pairs of columnar sites and 2 interstitial sites. The columnar sites lie evenly spaced along the bisectors of the faces of the unit

cell and can be thought of as forming three mutually perpendicular and interlocking columns. The interstitial sites fill out the space between the columns: one is at the center of the cell and the other one is at the vertex (Fig. 1).

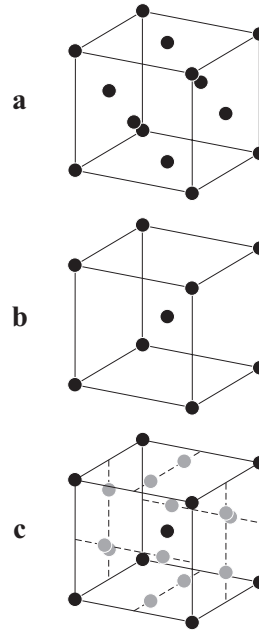


FIG. 1. Various lattices: (a) Face-centered cubic, (b) body-centered cubic, and (c) A15 lattices.

Though the structure of dendrimer crystals has been studied in great detail,<sup>17,18</sup> it remains unclear why the dendrimer assemblies should make the A15 lattice. The micelles are nearly spherically symmetric and very monodisperse:<sup>14</sup> given their chemical composition, the interaction between the micelles must be predominantly steric. If they were of uniform density, the interaction arising from the impenetrability of the micelles would be well-described by a spherically symmetric hard-core potential. In this case, one might expect the spheres to assemble into an FCC lattice to maximize their positional entropy – because it has the largest packing fraction, it maximizes the volume available to each sphere.<sup>11,12</sup> On the other hand, the A15 lattice is rather loosely packed, with the same packing fraction as that of the simple cubic (SC) lattice. Thus the A15 lattice is very inefficient from the point of view of the center-of-mass entropy of each sphere.

If the micelles were structureless hard spheres, their free energy would depend only on their position. However, the dendrimers have a well-defined structure consisting of a more or less compact core of benzyl ether rings and a floppy, squishy corona of alkyl chains. In this case, the stability of a certain arrangement of micelles does not depend only on the hard-core repulsion between the cores but also on the interaction between the brush-like coronas: the larger the overlap between the neighboring

micelles, the more constrained the conformations of the chains within the coronas and the smaller their orientational entropy (Fig. 2). This effective interaction is, of course, repulsive but short-ranged: at distances larger than the diameter of the micelles, their coronas do not overlap and the interaction vanishes.

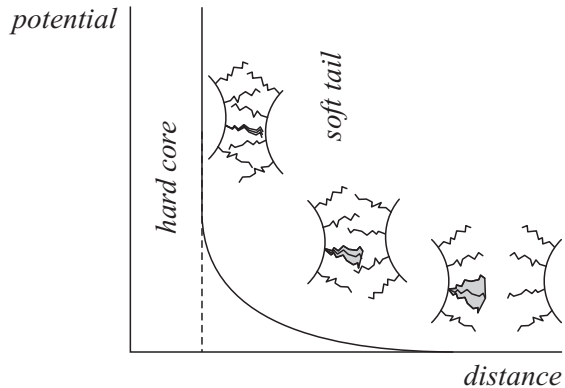


FIG. 2. Origin of the soft intermicellar potential: overlap between the micelles reduces orientational entropy of chains within the corona (shaded area), which gives rise to short-range repulsion.

Though the hard and the soft part of the repulsion both arise from the steric interaction between the dendrimers, their dependence on the density is very different. The hard cores lead to an inaccessible volume, while the matrix of interpenetrating soft coronas leads to a softer entropic repulsion. We can regard the matrix of coronas as a bilayer of dodecyl chains wrapped around each hard core. The free energy of these bilayers decreases monotonically with thickness. However, the volume of this soft matrix is fixed by the difference between the total volume and that of the hard cores and can be written as the product of the total area ( $A$ ) of these bilayers and their average thickness ( $d$ ), so that at a given density

$$Ad = \text{constant}. \quad (1)$$

Since the soft repulsion of the tails favors larger bilayer thicknesses  $d$ , the coronal entropy is maximized when the area  $A$  is minimized, or, in other words, when the interfacial area between the neighboring micelles is a minimal surface (Fig. 3). We should emphasize that the interface between the micelles is a mathematical concept that embodies the membrane-like, two-dimensional character of the interdigitated coronas, and it does not correspond to, say, the position of a particular segment of the dendrimer molecule.

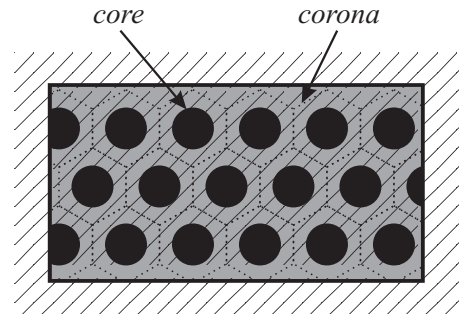


FIG. 3. A two-dimensional illustration of the minimal-area rule: the hard cores are embedded in the matrix of coronas, and the volume of the latter is given by the product of its area (dotted line) and the average separation of the cores.

It is essential to note that this minimal-area principle is incompatible with close packing and can favor lattices other than FCC, thereby giving rise to frustration in these systems and a rich phase diagram. If the free energy of the lattice of micelles depended only on the interfacial energy, the system would behave as periodic membrane enclosing bubbles of equal volume – as an ideal, dry soap froth. At this juncture the solution to the problem of minimizing the interfacial area of a set of equal volume, space-filling cells is not known. However, it is known that the area of the BCC “foam” is smaller than that of the FCC foam and that the A15 foam has a smaller area still.

### A. Kelvin’s problem

The problem of finding the ideal configuration of a soap froth was introduced by Kelvin in 1887 while studying how light propagated in a crystal, the relation being based on the now abandoned notion of aether. He realized that the dry soap froth problem could be cast in the mathematically precise form: What regular partition of space into cells of equal volume has the smallest area of cells? As is almost always the case, the plain and simple formulation of the problem is a harbinger of its complexity.

Kelvin built on Plateau’s investigations of the stability of soap films, summarized by two rules which represent mechanical equilibrium: In an equilibrium froth, (i) adjacent faces meet at an angle of  $120^\circ$  and (ii) the edges (the so-called Plateau borders) must form a tetrahedral angle of  $109^\circ 28'$ . It follows that arrangements with more than 3 faces meeting at a common edge are unstable as are junctions with more than 4 edges. At that time, these rules did not have a theoretical background and neither did Kelvin’s work. Kelvin’s approach relied on experiments based on soldered wire frames dipped into soap solution and the observation of the evolution of the soap film spanned by the frame.<sup>19</sup> Kelvin was led to the conclusion that his problem was solved by a lattice of polygons with the topology of an orthic tetrakaidecahe-

dron consisting of 6 quadrilateral and 8 hexagonal faces. In more modern terms these shapes are known as the Wigner-Seitz cell of the BCC lattice (Fig. 4). Kelvin subsequently worked out the exact shape of the faces and showed that to satisfy the Plateau rules, the edges of the tetrakaidehedra must be slightly curved and the hexagonal faces must be somewhat nonplanar.

Though a conjecture, Kelvin's partition of space was thought to be the solution of the problem by the mathematics community, despite the realization the proof might be highly elusive.<sup>20</sup> Indeed, these types of problems are notoriously difficult. For example, even the Plateau rules themselves were nothing but experimental facts until 1976 when they were put on a firm theoretical footing by Taylor<sup>21</sup> and it was only in 1999 that Hales proved that the regular hexagon is the solution of the two-dimensional variant of the Kelvin problem.<sup>22</sup> We also note that the related Kepler problem of packing hard spheres as densely as possible turned out to be equally challenging: the well-known FCC or HCP packing was demonstrated to be the most efficient in 1998, the proof being furnished again by Hales.<sup>12</sup>

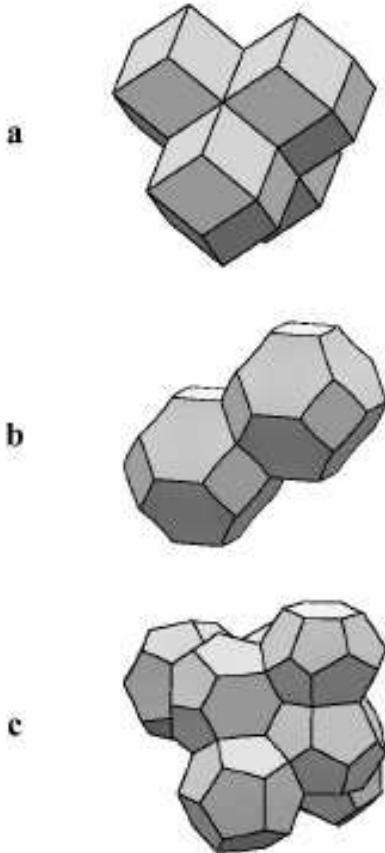


FIG. 4. Rhombic dodecahedron/FCC lattice (a), Kelvin's tetrakaidehedron/BCC lattice (b), and Weaire-Phelan minimal surface/A15 lattice (c).

Kelvin's conjecture stood unchallenged for more than a century until 1994 when Weaire and Phelan discovered that a froth with the symmetry of the A15 lattice has an area smaller than BCC lattice by 0.3%.<sup>23</sup> While this may seem to be a small difference, it is, in fact, significant: the relative difference in the areas of Kelvin's BCC structure and the FCC-type partition of rhombic dodecahedra (unstable as a froth because it contains vertices joining 8 edges) is 0.7%. Thus the A15 foam is a 50% improvement on this scale.

The A15 foam consists of 6 Goldberg tetrakaidehedra, each with 2 hexagonal and 12 pentagonal faces, which form three sets of interlocking columns, and 2 irregular pentagonal dodecahedra at the interstices. Since it is composed of two types of cells, the Weaire-Phelan soap froth is obviously less symmetric than Kelvin's froth. However, it was not surprising to some that it has a rather small surface area. The A15 lattice is derived from the polytope  $\{3, 3, 5\}$ , a partition of positively curved space consisting of 120 regular dodecahedral bubbles. As suggested by Kléman and Sadoc, positive spatial curvature relieves the frustration brought about by the incompatibility of the optimal local arrangement of bubbles and the structure of flat three-dimensional space. The polytope  $\{3, 3, 5\}$  should be regarded as the ideal template whence the various tetrahedrally close-packed (TCP) lattices (the layered TPC lattices are also known as Frank-Kasper phases) are derived via decurving, *i.e.*, by substituting some of the dodecahedral cells by bubbles with 14 (= 12 pentagonal + 2 hexagonal), 15 (= 12 pentagonal + 3 hexagonal), or 16 (= 12 pentagonal + 4 hexagonal) faces.<sup>13,24,25</sup> Cells with 13 faces are forbidden for topological reasons, and those with more than 16 faces are dynamically unstable.<sup>13</sup>

There are 24 known ways of decurving the polytope  $\{3, 3, 5\}$  and thus 24 TCP crystal lattices.<sup>13</sup> With 2 types of bubbles and 8 bubbles per unit cell, the A15 lattice is among the simplest: the unit cell of the most complicated structure, the so-called I lattice, consists of 228 bubbles that include all 4 types of bubbles.<sup>13</sup> Given the rationale for the success of the A15 lattice, it is not unreasonable to expect that other TPC lattices may have an even smaller surface area. Indeed, the discovery of Weaire and Phelan renewed the interest in the field. Subsequently some of the remaining TCP-type soap froths have been studied,<sup>26</sup> facilitated by Surface Evolver, a remarkable software package developed by Brakke.<sup>27</sup> In addition, other classes of periodic and quasiperiodic partitions based on Kelvin's BCC and Williams' body-centered-tetragonal (BCT) bubbles have been suggested.<sup>28</sup> At this time, however, the A15 foam has not been bested – it stands as the tentative solution of Kelvin's problem.

The connection between the observed crystal structure and the soft part of the intermicellar potential should now be clear: if it were absent, the hard cores would favor an FCC lattice, but instead the equilibrium structure is a different lattice with a larger bulk free energy but a smaller surface free energy. The only variables in

this model are the parameters of the surface interaction, which we will estimate roughly. In view of the experimental data on soft spheres, we will compare the FCC, BCC, and A15 lattices and show that in the case of the dendrimer micelles, it is reasonable to expect that the area-minimizing A15 lattice is favored over the close-packed FCC lattice.

## B. Bulk free energy

Within the framework of the two competing ordering principles, we propose a simple and approximate theory of colloidal crystals where the bulk and the surface terms are coupled only through the constraint of fixed volume. As far as the bulk free energy is concerned, the micelles will be treated as hard spheres of diameter  $\sigma$ , and the surface interaction will be calculated as if the matrix of coronas were a thin structureless layer so that we may neglect the effects of curvature.

We start our analysis with the bulk term. The configuration integral of a one-component classical system of  $N$  particles confined to a volume  $V$  is

$$Z = \frac{1}{\lambda^{3N} N!} \int_V \prod_{i=1}^N d\mathbf{r}_i \exp(-U(\mathbf{r}_1, \mathbf{r}_2, \dots, \mathbf{r}_N)/k_B T), \quad (2)$$

where  $\lambda = \sqrt{\hbar^2/2\pi m k_B T}$  is the thermal de Broglie wavelength and  $U(\mathbf{r}_1, \mathbf{r}_2, \dots, \mathbf{r}_N) = \frac{1}{2} \sum_{i,j=1}^N u(\mathbf{r}_i, \mathbf{r}_j)$  is the total interaction energy consisting of pairwise interactions  $u(\mathbf{r}_i, \mathbf{r}_j) = u(|\mathbf{r}_i - \mathbf{r}_j|)$ . Despite the simplicity of the hard-core potential,  $Z$  cannot be calculated analytically, and one must resort either to numerical approaches, such as Monte Carlo simulations, or to approximate analytical methods. The latter are more appropriate for our purposes since we are seeking a simple, heuristic explanation of crystal structure. When considering crystal phases we can assume that the particles are localized within cells formed by their neighbors and thus the configuration integral breaks up into  $N$  single-particle integrals so that

$$Z \approx \left( \lambda^{-3} \int_{V_0} d\mathbf{r} \exp(-u_{\text{eff}}(\mathbf{r})/k_B T) \right)^N, \quad (3)$$

where  $V_0$  is the volume of the cell (usually the Wigner-Seitz cell),  $u_{\text{eff}}(\mathbf{r})$  is the effective potential felt by the particle, and  $N!$  has been absorbed by factorization of the partition function. This approximation is valid only for lattices where all sites are equivalent; if the unit cell of the crystal consists of inequivalent sites, Eq. (3) can be embellished accordingly.

As natural as this approximation may seem for a periodic arrangement of particles in a crystal, it neglects any correlated motion of neighbors and the associated communal entropy.<sup>29,30</sup> Nevertheless, the cellular model

often gives quantitatively accurate results that are in good agreement with more complete numerical simulations. For hard spheres, where the cellular theory becomes exact in the high-density limit, the agreement with Monte Carlo results is in fact excellent.<sup>30,31</sup> In this case, each particle is assumed to be uniformly smeared over its reduced Wigner-Seitz so that it cannot overlap with its neighbors. As a result, the effective potential is quite simple: 0 within the volume the center of mass is allowed to trace out (the so-called free volume) and infinite otherwise. Thus

$$Z \approx \left( \lambda^{-3} \int_{V_F} d\mathbf{r} \right)^N = (V_F/\lambda^3)^N, \quad (4)$$

where  $V_F$  is the free volume whose shape reflects the symmetry of the lattice.<sup>30</sup> We note that temperature drops out of this problem and that the interaction is entirely entropic.

Within the cellular free-volume theory, the free energy of hard spheres becomes a purely geometrical issue. All one has to do is to calculate the volume of the Wigner-Seitz cell after a layer of thickness  $\sigma/2$  has been peeled off of its faces, which is the volume accessible to the particle's center of mass. In the FCC lattice, the free volume has the shape of a rhombic dodecahedron just as the Wigner-Seitz cell.<sup>32</sup> On the other hand, in the BCC lattice it remains an orthic tetrakaidecahedron only at rather low densities far below the freezing point. At higher densities, where the hard spheres form a solid phase, the square faces become absent rendering the free volume a regular octahedron. For the FCC and BCC lattices, the bulk free energy per dendrimer micelle reads

$$F_{\text{bulk}}^X = -k_B T \ln \left( \alpha^X \left( \frac{\beta^X}{n^{1/3}} - 1 \right)^3 \right), \quad (5)$$

where  $X$  stands for FCC or BCC,  $n = \rho\sigma^3$  is the reduced number density ( $\sigma$  being the hard-core diameter), and the term  $-3k_B T \ln(\sigma/\lambda)$  which is independent of the lattice structure has been dropped. The coefficients  $\alpha^{\text{FCC}} = 2^{5/2}$  and  $\alpha^{\text{BCC}} = 2^2 3^{1/2}$  reflect the shape of the free volume, and  $\beta^{\text{FCC}} = 2^{1/6}$  and  $\beta^{\text{BCC}} = 2^{-2/3} 3^{1/2}$  specify their size.

The free volume of the A15 lattice, which includes two types of sites, is a bit more complicated. As determined by the Voronoi construction subject to the constraint that all cells have equal volume, the shapes of the free volumes are irregular pentagonal dodecahedra and tetrakaidecahedra with two hexagonal and twelve pentagonal faces rather than regular polyhedra. Their volumes cannot be expressed in an amenable analytical form, and thus we have calculated them numerically for a range of densities. However, we note that the exact free volumes can be approximated very well by replacing the dodecahedra and tetrakaidecahedra by spheres and cylinders, respectively (Fig. 5).

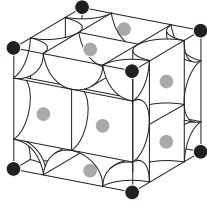


FIG. 5. Approximate analytical model of the bulk free energy for the A15 lattice: free volumes of columnar and interstitial sites are replaced by cylinders and spheres, respectively.

This *ansatz* takes into account that the free volume of a columnar site changes anisotropically with density and approaches a flattened shape in the close-packing limit, whereas the shape of the free volume of interstitial sites does not depend on density. We also introduce two adjustable parameters that quantify the fact that the actual volumes of the Wigner-Seitz cells are larger than the volumes of spheres and cylinders, which leave empty voids between them. Given that the ratio of columnar and interstitial sites is 3:1, this leads to the average bulk free energy per micelle of

$$F_{\text{bulk}}^{\text{A15}} = -k_B T \left[ \frac{1}{4} \ln \left( \frac{4\pi S}{3} \left( \frac{\sqrt{5}}{2n^{1/3}} - 1 \right)^3 \right) + \frac{3}{4} \ln \left( 2\pi C \left( \frac{\sqrt{5}}{2n^{1/3}} - 1 \right)^2 \left( \frac{1}{n^{1/3}} - 1 \right) \right) \right]. \quad (6)$$

This formula best agrees with the numerical results for  $S = 1.638$  and  $C = 1.381$ , where the relative deviation from the true bulk free energy is below 0.1% at densities higher than  $n \approx 0.8$  and not significantly larger at lower densities.  $F_{\text{bulk}}^{\text{FCC}}$ ,  $F_{\text{bulk}}^{\text{BCC}}$ , and  $F_{\text{bulk}}^{\text{A15}}$  are plotted in Fig. 6.<sup>15</sup>

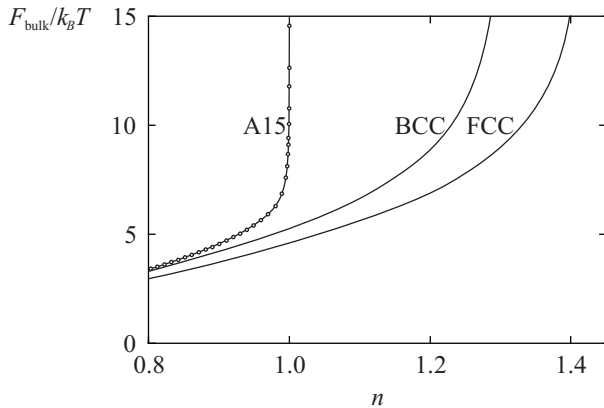


FIG. 6. Bulk free energies of hard-core particles arranged in FCC, BCC, and A15 lattice as calculated with the free-volume theory. Solid lines correspond to Eqs. (5) and (7), and circles are numerical results.

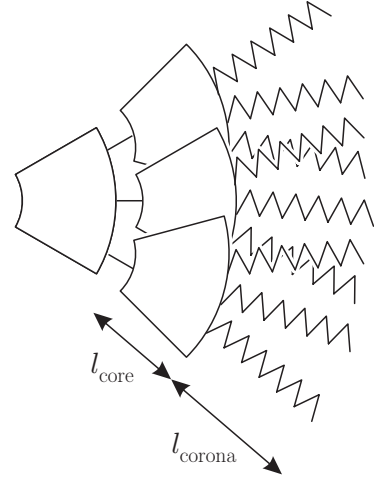


FIG. 7. Structure of dendrimers that form the A15 lattice: 1st generation dendrimer consists of a core segment and three dodecyl chains, 2<sup>nd</sup> generation dendrimer includes three 1<sup>st</sup> generation dendrimers attached to a core segment, and so on. The length of the core segment and the dodecyl tail is  $l_{\text{core}} = 0.6$  nm and  $l_{\text{corona}} = 1.4$  nm, respectively. Shown here is a 2<sup>nd</sup> generation dendrimer.

### C. Surface free energy

Having calculated the bulk free energy for the three lattices, we now turn to the surface free energy, which requires a specific model of the soft interaction between the particles. To determine which model is the most appropriate, we should first find out whether the overlap of the neighboring particles is large or small. At this point, the analysis becomes somewhat less general, because the overlap differs from one system to another. Being interested primarily by the stability of the loosely-packed crystal lattices, we now focus on the dendrimers that form the A15 crystal.<sup>14</sup> The relevant quantitative data include measurements of the radii of dendrimer molecules and the lattice constants of the micellar crystals. Since the dendrimers consist of 2, 3, or 4 generations of branching benzyloxy segments crowned by dodecyl chains with bare radii of  $\sigma_{\text{bare}}/2 = 2.6, 3.2,$  and  $3.8$  nm, respectively, we can deduce that the lengths of the benzyloxy core segment and the dodecyl chain are  $l_{\text{core}} = 0.6$  nm and  $l_{\text{corona}} = 1.4$  nm (Fig. 7). The effective diameter of the micelles  $\sigma_{\text{eff}}$  can be calculated from the lattice constant  $a$ . According to Fig. 1,  $\sigma_{\text{eff}} = a/2$ . This gives  $\sigma_{\text{eff}} = 3.4, 4.0,$  and  $4.2$  nm. Obviously,  $\sigma_{\text{eff}}$  is considerably smaller than  $\sigma_{\text{bare}}$  for all generations. Actually, the most conclusive information can be extracted from 4<sup>th</sup> generation data: 2<sup>nd</sup> and 3<sup>rd</sup> generation micelles probably have an empty center and their true diameter is most likely larger than  $\sigma_{\text{bare}}$ . These data show that the effective diameter of the hemispheric 4<sup>th</sup> generation micelles,  $4.2$  nm, does not exceed the diameter of their benzyloxy core,  $8l_{\text{core}} = 4.8$  nm. Thus we can conclude that the hard-core

diameter of the monodendrons must be smaller than the diameter of the benzyloxy core. Thus not only is there a considerable overlap between the coronas, but also the dodecyl chains penetrate into the core itself. This indicates that the interfacial effects, related to the limited orientational entropy of the chains, are important in the dendrimer system.

In the absence of a quantitative insight into the intermicellar potential – such as a direct measurement of the interaction via optical trapping<sup>33</sup> – we model the interaction of the interpenetrating dodecyl chains as the interaction between grafted polymer brushes.<sup>34</sup> In the high-interdigitation limit, which is certainly applicable in our case, the free energy of a compressed brush reduces to the excluded-volume repulsion of the chains. An argument in the spirit of Flory theory gives

$$F_{\text{surf}} = \frac{\ell N_0 k_B T}{h} = \frac{2\ell N_0 k_B T}{d}, \quad (7)$$

where  $\ell$  is a parameter with the dimension of length, which determines the strength of repulsion,  $N_0$  is the number of chains per micelle, and  $h$ , the thickness of the single corona, is half the average thickness of the interdigitated matrix of the chains  $d$ . This approximation neglects some details of the actual interaction, most notably the curvature of the dodecyl brushes in the coronas. However, these effects are subdominant when the dendrimers are packed very closely. In fact, it is known that the density is nearly constant in the volume occupied by the chains,<sup>14</sup> and we thus expect that our model should provide a robust description of the system.

The thickness  $d$  of the coronal matrix depends on the density since the dodecyl bilayer must fill the space between the hard cores.<sup>15</sup> Thus

$$d = \frac{2(n^{-1} - \pi/6)\sigma^3}{A_M}, \quad (8)$$

where  $A_M$  is the interfacial area per micelle. Since the area is proportional to the square of the lattice constant, the surface free energy per micelle reads

$$F_{\text{surf}}^X = \frac{\ell N_0 k_B T}{\sigma} \frac{\gamma^X n^{-2/3}}{n^{-1} - \pi/6}, \quad (9)$$

where  $\gamma^X$  is the coefficient determined by the symmetry of the lattice and defined by  $A_M = \gamma^X \sigma^2 n^{-2/3}$ . Lower values of  $\gamma^X$  correspond to more area-efficient partitions. The typical magnitude of this coefficient is set by the simple cubic (SC) lattice, which gives  $\gamma^{\text{SC}} = 6$ . The more efficient area-minimizing lattices have smaller values of  $\gamma^X$ :  $\gamma^{\text{FCC}} = 25/63 = 5.345$ ,  $\gamma^{\text{BCC}} = 5.306$ , and  $\gamma^{\text{A15}} = 5.288$ .<sup>23</sup>  $\gamma^{\text{BCC}}$  and  $\gamma^{\text{A15}}$  can only be computed numerically, e.g., using Surface Evolver.<sup>27</sup> As a comparison, the ultimate lower bound for  $\gamma$  corresponds to a sphere (which, of course, is not a space-filling body):  $\gamma^{\text{sphere}} = 2^{2/3} 3^{2/3} \pi^{1/3} = 4.836$ .

Combining Eqs. (5), (7), and (9), we arrive at a single-parameter ( $\ell$ ) free energy of micellar crystals:

$$F^X = F_{\text{bulk}}^X + F_{\text{surf}}^X. \quad (10)$$

Before we calculate the minimal strength of the soft repulsion necessary to stabilize the area-minimizing structures, we need to determine the density of the crystal. Not knowing the hard-core radius of the micelles, we can only provide an order-of-magnitude estimate of  $\ell$ , and for this purpose, it is sufficient to note that unless the observed A15 lattice approaches the packing limit of  $n = 1.0$ , its bulk free energy per micelle is roughly  $1k_B T$  larger than  $F_{\text{bulk}}^{\text{BCC}}$  and  $2k_B T$  larger than  $F_{\text{bulk}}^{\text{FCC}}$ . To be concrete, we compare the total free energies at  $n = 0.95$ , which is well within the high-density regime but not quite at the close-packing limit and thus consistent with the structural data. At this density, the BCC lattice becomes more favorable than FCC at  $\ell \gtrsim 0.05\sigma$  whereas the BCC-A15 transition occurs at  $\ell \approx 0.15\sigma$ . Given that there are  $N_0 = 162$  dodecyl chains per 3rd and 4th generation micelle, these values of  $\ell$  correspond to an entropy of about  $0.5k_B$  and  $1.5k_B$  per chain, respectively. In other words, this means that if the overlap of the micelles is so large that the decrease of orientational entropy of a chain due to interdigitation reaches  $0.5k_B$  and  $1.5k_B$ , the differences between the surface entropies of the BCC and FCC lattices and the A15 and BCC lattices overcome the corresponding differences of the bulk entropies and thus favor the area-minimizing structures.

These values are physically reasonable and of the correct order of magnitude. When unrestricted by other chains, each chain has a few orientational and conformational degrees of freedom. Thus its entropy is a few  $k_B$ , and so it can easily lose  $0.5k_B$ ,  $1.5k_B$ , or more entropy upon interdigitation. If we plug these numbers back into the free energy, we learn one more thing about these systems: their energetics is controlled primarily by the surface term, which is a direct consequence of the three center-of-mass degrees of freedom associated with the hard cores being greatly outnumbered by the several hundreds of internal degrees of freedom associated with the dodecyl chains. In other words, in the dendrimer system the “squishiness” of the particles wins over their hard cores.

#### D. A new paradigm

Our proposed model provides a novel way of looking at the self-organization of colloidal crystals. By complementing the well-known close-packing rule, which controls the stability of hard spheres, with the minimal-area rule, which stems from the additional short-range repulsion between the particles, we have shown that the equilibrium ordered structures are a result of frustration between two incompatible requirements. This picture implies that if the corona is thin compared to the core, the colloids will behave as hard spheres and form a close-packed lattice such as FCC, but as it grows thicker, an area-minimizing structure – the A15 lattice – should be

observed. In between the two extremes, there may be a spectrum of lattices that neither maximize the packing fraction nor minimize the interfacial area but represent a reasonable compromise for a given intermicellar potential. However, in some systems coexistence of the FCC and A15 lattices could be energetically preferable to an intermediate structure such as BCC, provided that the density is not too high to destabilize the A15 lattice.

This observation is consistent with the experimentally determined structures found in other colloidal materials, such as crystals of aurothiol particles consisting of a gold crystallite core and covered by about 50  $n$ -alkylthiols where  $n = 4, 6, \text{ or } 12$ . This system is remarkably close to the dendrimer system in both size and structure. The diameter of the metallic cores can be varied from 1.6 to 3.1 nm, and the length of the (fully extended) coronal chains is between 0.6 to 1.56 nm. The alkylthiol chains were adsorbed to the gold core with the sulfur atom, leaving the outer part of the corona chemically identical to the dendrimer coronas. Depending on the relative size of the corona with respect to the diameter of the core, either the FCC or BCC lattice was observed. In addition, in some samples the BCT lattice was found as a moderately anisotropic variation of the BCC lattice with  $c/a \sim 1.15$ . (We will see later on that this lattice is not really unexpected although it departs somewhat from our model: in a BCT crystal, both the bulk and surface entropy are larger than their BCC counterparts.)

A particularly interesting feature of this system is that the size of the core can be varied continuously, so that the FCC-BCC transition can be located very precisely. For the range of core radii explored in the study,<sup>35</sup> an FCC-BCC transition was found in particles covered with hexylthiol chains: the FCC lattice is stable if the ratio of the thickness of corona and the core radius is smaller than about 0.73, and BCC or BCT lattices are observed otherwise. The structural parameters of the aurothiol particles were measured in some detail and if we identify the hard core with the gold nanocrystal, we find that the reduced density at the transition is about  $n_{\text{FCC-BCC}} = 0.4$ . Proceeding along the same lines as before, this gives an entropy decrease of about  $0.05k_B$  for each of the approximately 150 chains in the corona. Although still reasonable, this estimate is by an order of magnitude smaller than in the dendrimer case. However, we note that because of the high coverage of the gold cores with the adsorbed alkylthiols, the effective hard-core diameter of the particles is most likely larger than the gold core diameter. In this case, the reduced density at the transition would be larger, and this would lead to a larger entropy decrease per alkylthiol chain. Nonetheless we can still combine this figure with its dendrimer counterpart to bound the value of the entropy per coronal chain at the FCC-BCC transition between 0.05 and  $0.5k_B$ , which can serve as an estimate for future studies.

Similar behavior was discovered in polystyrene-polyisoprene diblock copolymers dispersed in decane, a solvent preferential for the polyisoprene.<sup>36,37</sup> These di-

blocks spontaneously form micelles with a polystyrene core and polyisoprene corona. Indeed, micelles based on diblocks with a core segment containing from 1.5 to 2 times as many monomers as the coronal segment crystallize into an FCC lattice.<sup>37</sup> On the other hand, in copolymers made of blocks with the same number of monomers the BCC lattice was observed. Although the A15 lattice was not seen in this system, we conjecture that it could be found in copolymers with the polyisoprene block sufficiently longer than the polystyrene block.

While rare in crystalline systems, we mention that the A15 structure is not uncommon in lyotropic systems, typically containing lipids dispersed in water matrix. These systems self-arrange in either direct or inverted micelles, which are known to form a variety of cubic structures.<sup>38-41</sup> However, the existence of the A15 lattice in lyotropic systems should not be as surprising as in colloidal systems. The cohesive force of these micelles is the hydrophobic interaction which means that their size is not as well-defined as in colloids. If there can be several types of micelles the A15 lattice is not hard to assemble. The other difference with respect to colloids is that the water matrix that encloses the micelles is truly fluid and thus much more similar to actual wet soap froths with relatively large liquid content. At the same time, in the lyotropic systems the effective intermicellar potential may not be necessarily dominated by steric effects, implying that the stability of a particular ordered micellar structure can depend on the chemical composition of lipids.

Specific effects like these can not easily be incorporated into our framework: our goal was not to develop an elaborate description that would cover the many details that are captured in more or less involved theories, such as self-consistent field theory<sup>42</sup> and various Monte Carlo schemes.<sup>10,43</sup> Instead, we have proposed a heuristic model that describes the essential physics of many colloids and clearly exposes the frustration that is introduced by dressing hard spheres with a soft repulsive interaction. This model provides an explanation of the results of the more rigorous theories with the added advantage that it is very simple, yet can give reasonable semiquantitative predictions about the stability of the different lattices. Obviously, it can be improved by introducing a more refined model of the interfacial interaction which would account for the curvature of the coronal matrix, the strain of the coronas into the interstitial regions, solvent effects, and related phenomena.

As useful as it might be, like all coarse-grained approaches, the proposed theory<sup>15</sup> has some limitations. Our model is tailored for a broad yet specific class of colloidal particles that interact by short-range potentials, and it may not be suitable for systems characterized by long-range forces, such as unscreened or partly screened electrostatic forces. The range of potential is determined by the requirement that the nearest-neighbor interaction be much stronger than the interaction with the rest of the particles; otherwise we could not define the concept

of the interface. Additionally, we have decoupled the bulk and interfacial free energies, or the hard and soft parts of the potential. We suspect that a limit of the full problem exists in which the minimum-area principle is a mean-field approximation.

In order to gain insight into colloidal crystal structure and to strengthen the case for our new principle, we will, in the next Section, calculate the phase diagram for a certain interparticle potential, and identify the range of stability of the A15 lattice using a “single-particle” Monte Carlo algorithm. The significance of these results is twofold: at the qualitative level, they suggest that the phase diagram of soft spheres can include a variety of solid phases, not just FCC and BCC lattices, and at the quantitative level they will provide guidance for a more complete numerical analysis of the system.

### III. SHORT-RANGE POTENTIALS AND SOLID-SOLID PHASE TRANSITIONS

#### A. Crystal architecture

The FCC lattice, which, as we know now for certain,<sup>12</sup> is the closest regular packing of hard spheres with cubic symmetry, with each site enclosed completely by the 12 equidistant neighbors. In the case of a purely hard core interaction, the free energy consists solely of the entropic contribution and is a convex function of volume. To model the effect of the soft coronas in the systems we are discussing, we add to the hard core a soft potential of range  $\delta$ . Note that we are replacing an entropic interaction with an energetic term which should make no difference to our argument but is more convenient in our calculational scheme. At densities low enough so that the average distance between the particles is much larger than  $\delta$ , the overlap of the coronas is small and so the free energy is dominated by the entropy, as if the extra potential were not there. On the other hand, in the high-density limit where the separation between the hard cores is smaller than  $\delta$ , each particle feels the soft potential of all neighbors. If the potential is flat enough, the average field may in fact not change dramatically with position and then the particle will behave essentially as if it were a hard sphere moving in a constant potential, its free energy being given by the entropic contribution of the hard-core interaction shifted by the energy of the overlapping coronas. For certain forms of the soft potential, the transition from the low-density to high-density regime can be rather abrupt (Fig. 8). Upon compression, the free energy of the colloid will then change quite sharply and may no longer be a convex function of volume. In this case, the low-density and high-density behavior will be separated by a region of coexistence between expanded and condensed FCC lattices, implying an isostructural transition between them.<sup>8</sup>

Coexistence between the expanded and condensed FCC phases is not the only possibility: other crystal lattices may exist in this density regime where it may be favorable for the spheres to be configured in a structure with a somewhat higher entropy but lower energy. For example, the BCC lattice has a more open architecture compared to FCC where the “cage” of each particle is defined by the 12 nearest neighbors. In the BCC lattice, the 8 nearest neighbors do not enclose the particle completely: as the Wigner-Seitz cell shows us, even in the hard-core limit, each particle also interacts with the 6 next-to-nearest neighbors. At any fixed density, the 8 neighbors from the first coordination shell are closer to the particle than in the FCC crystal, but the 6 second-shell neighbors are further away. As a result, BCC hard spheres have a lower entropy than the FCC hard spheres, but the additional soft potential can stabilize the BCC lattice. The more structured arrangement of sites implies that upon compression, the energy of the BCC crystal increases more gradually than its FCC counterpart: the central particle first overlaps with the first-shell neighbors alone and in this density regime the BCC free energy can be lower than the free energy of the coexisting expanded and condensed FCC phases, provided that the soft potential overlaps with all 12 neighbors of the FCC lattice. At somewhat higher densities the particles in the BCC lattice interact with all of the 14 neighbors and then both the entropic and energetic terms disfavor the BCC lattice. Similarly, the stability of the A15 lattice and other more structured phases is facilitated by their even smoother, less step-like free energy as a function of volume.

This view of the energetics is closely related to the structure of the pair distribution function of a particular lattice. As long as the interaction between the particles is short-range, one only has to consider the pair distribution function at short separations, which directly reflects the shape of the corresponding Wigner-Seitz cell. If the distribution function has a single peak as in the highly symmetric FCC crystal, a soft short-range repulsion between the particles can destabilize the lattice with respect to other lattices with more complex pair distribution functions. As noted above, these include the BCC lattice with two peaks at short distances (Fig. 9) but also the anisotropic variants such as the BCT lattice<sup>35</sup> where the 6 BCC second-shell sites are split into a subshell of 4 sites and a subshell of 2 sites, and the BCO lattice<sup>10</sup> where the fourfold BCT next-to-nearest-neighbor subshell is further split in two subshells. (Curiously, the anisotropic version of the FCC lattice – the face-centered orthorhombic (FCO) structure has not yet been observed in a colloidal or related system.)

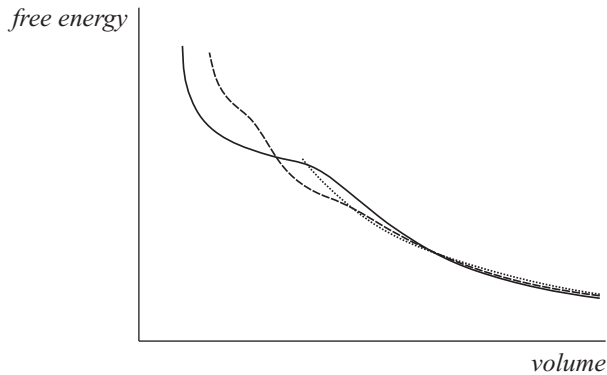


FIG. 8. Schematic of the free energy profile for a model hard-core-soft-shoulder potential. The short range of the shoulder makes the free energy a nonconvex function of volume, and thus induces either isostructural or structural transitions in the solid phase. Solid line: FCC; dashed line: BCC; dotted line: A15.

This argument can be extended to include other, less symmetric lattices. An example is the A15 lattice. By considering the pair distribution function, we see that, on average, each site interacts with 13.5 neighbors: through the faces of their Wigner-Seitz cells, the columnar and interstitial sites interact with 14 and 12 neighbors, respectively, and there are 3 times as many columnar sites as the interstitial sites. Of these 13.5 neighbors, 1.5 particles are closest to the central particle, followed by two shells of 6 particles at larger distances (Fig. 9). While it is obvious that this lattice must have a smaller entropy than BCC, for a suitably chosen soft potential it could have a lower net free energy. An extreme case of the tradeoff between entropy and energy is the diamond phase observed in a numerical study of packing of star polymers which interact with an extremely soft potential.<sup>10</sup> The diamond lattice with 4 nearest and 12 next-to-nearest neighbors is clearly unfavorable from the entropic point of view, but apparently the pair distribution function is so strongly peaked at next-to-nearest neighbors that for certain types of short-range interparticle potentials the energy of the diamond lattice is very low.

While these ideas provide additional perspective and complement our foam model described above, it is not completely clear whether the structural characteristics captured by the pair distribution function can be easily related to the minimal-area principle and Kelvin problem. We will not pursue this interesting question here; instead, we now turn to statistical mechanics of soft spheres.

## B. Phase diagrams

The phase behavior of soft-sphere systems has had ongoing study over the years. A variety of purely repulsive forces have been considered, including power law potentials as the high-temperature limit of the van der

Waals interaction,<sup>44</sup> screened Coulomb potentials with<sup>45</sup> or without a hard core,<sup>5,4</sup> and square shoulder potentials<sup>8,7,46</sup> as well as their variants.<sup>47</sup> With its flat plateau and as sharp a cutoff as possible, the square-shoulder potential is very sensitive to the structure of the pair distribution function and thus the quintessential short-ranged interaction. This is the reason why it is used so often to analyze solid-solid transitions. We shall use the square-shoulder interaction in the following, in order to provide a comparison with earlier studies.

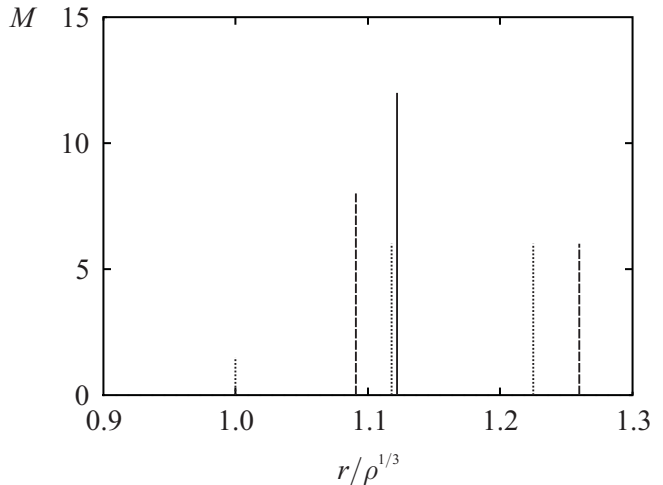


FIG. 9. Structure of the FCC (solid line), BCC (dashed line), and A15 lattice (dotted line) represented by the radii of a few nearest coordination shells weighted by the corresponding coordination number  $M$ . (If peaks were multiplied by  $\delta$ -functions, this would be the  $T = 0$  pair distribution function integrated over the solid angle.) FCC is the most closed lattice, each particle having 12 equivalent neighbors, whereas BCC and A15 are more open structures with 2 and 3 inequivalent neighbor sites, respectively.

The hard-core square-shoulder (HCSS) system is characterized by a pairwise potential of the form

$$u(r) = \begin{cases} \infty & r < \sigma \\ \epsilon & \sigma \leq r < \sigma + \delta \\ 0 & r > \sigma + \delta \end{cases} \quad (11)$$

where  $\delta$  and  $\epsilon > 0$  are the thickness and the height of the shoulder, respectively (Fig. 10). This system has already been studied<sup>7,48</sup> by using density-functional perturbation theory, which treats the behavior of the system primarily by the hard-core interaction and treats the additional soft potential as a perturbation. If the free energy and the structure of the reference state ( $F_{\text{ref}}$ ) are known, the total free energy may be expanded to linear order in the perturbative term<sup>49</sup>:

$$F[\rho(\mathbf{r})] = F_{\text{ref}}[\rho(\mathbf{r})] + \frac{1}{2} \int d\mathbf{r}_1 d\mathbf{r}_2 \rho_{\text{ref}}^{(2)}(\mathbf{r}_1, \mathbf{r}_2) \phi(r_{12}), \quad (12)$$

where  $\mathbf{r} = \mathbf{r}_2 - \mathbf{r}_1$  describes the relative position of the two particles,  $\rho_{\text{ref}}^{(2)}(\mathbf{r}_1, \mathbf{r}_2)$  is the pair distribution function of the reference state, and  $\phi_{\text{pert}}$  is the perturbative part of the potential. The inputs of this scheme are the pair distribution function and the free energy of the reference system. Typically, the free energy of the solid HC phases are described within the so-called cellular free volume theory<sup>30,29</sup> and the corresponding pair distribution is calculated from the Gaussian one-particle density, whereas the fluid free energy and pair distribution are described by the Carnahan-Starling formula and the Verlet-Weis formula, respectively.<sup>49</sup>

Within perturbation theory, it has been found that the solid part of the phase diagram can indeed be very complex, and that its topology depends very delicately on

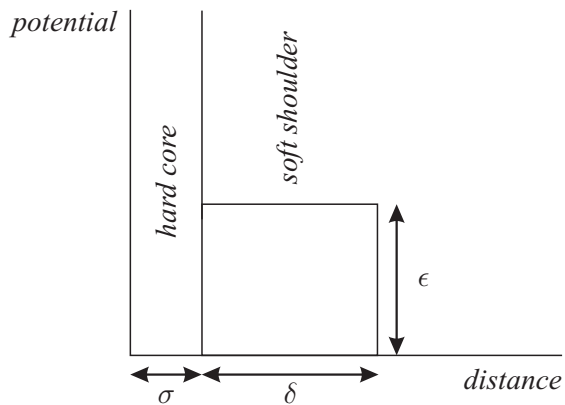


FIG. 10. Hard-core-soft-shoulder potential

the parameters of the potential. For relatively narrow shoulders, the phase diagram differs from its hard-core counterpart only in the expanded FCC–condensed FCC transition that occurs at densities near the close-packing density and terminates at a critical point. As the shoulder becomes broader, the region of coexistence between the expanded and condensed phases shifts towards lower densities. Eventually, the expanded FCC structure is replaced in part by the BCC at intermediate temperatures, *i.e.*, at temperatures high enough so that the shoulder does not appear very high, yet low enough so that it is not irrelevant. According to this analysis, the transition between the fluid and condensed FCC phase can be either direct or indirect, the intervening phases being BCC, expanded FCC, or both. Similar results were obtained for a sloped shoulder and a square shoulder followed by a linear ramp, except that these potentials give rise to several new features of the phase diagram, such as the expanded BCC–condensed BCC transition and a triple point. These predictions are consistent with the limited Monte Carlo results available,<sup>8</sup> but most of the features remain to be verified by rigorous numerical studies.

The perturbation analysis has provided valuable information on the behavior of HCSS spheres, but its pre-

dictive power is limited to high temperatures where the expansion is valid. Although some additional information can be obtained by interpolating between the high-temperature and zero-temperature data, this leaves out the most interesting part of the phase diagram. A natural extension of this approach is to calculate the configuration integral nonperturbatively. This can be done, for example, within a mean-field approximation in the cellular model where each particle is assumed to move independently in the average field of its neighbors. Such an approximation can be used within the cellular model by assuming an appropriate *ansatz* for the probability density – usually a sum of Gaussians – which then leads to a self-consistency relation determined by the requirement that probability densities of all particles be the same, thereby fixing the parameters of the *ansatz*.<sup>4</sup> Here we follow the spirit of this approach but we note that in the case of a system interacting with flat potential such as HCSS, the Gaussian *ansatz* may not be adequate. Moreover, in the A15 lattice the probability distribution of particles in columnar positions should be very anisotropic and in fact nonspherical. Given that our main task here is to examine the possibility that the phase diagram of the HCSS system includes the A15 lattice, it seems appropriate to capture the geometrical details of the different structures by calculating the configuration integral numerically.

Our procedure places the central particle within a cage of its neighbors that are themselves allowed to sample a distribution of positions such that the probability densities of all particles at equivalent sites are the same. This is achieved by sampling the actual probability density of the central particle continuously, and recreating identical distributions at the equivalent neighbor positions.<sup>50</sup> After equilibrating the system for a certain number of steps and checking for the consistency of the distributions of the central particle and the neighbors, we calculate the configuration integral and the free energy. This approach could be dubbed a “single-particle Monte Carlo method”; we note, however, that it is in fact a numerical variant of the self-consistent mean-field approximation and a relative of the variational method proposed by Kirkwood<sup>51</sup> rather than a simplified variant of a true multiparticle Monte Carlo integration. Our procedure is single particle because we approximate the multiparticle probability density by a product of single-particle probability densities and thus ignore long-wavelength excitations.

To ensure that the model reduces to the quantitatively successful cellular free-volume theory used in Section II<sup>31</sup>, we modify the HCSS interparticle potential by not allowing the hard core of the particle to leave the cell. This gives the correct free energy for small shoulders, ( $\epsilon < k_B T$ ) in good agreement with Monte Carlo analyses,<sup>7,48</sup> as well as for large shoulders, where the particles behave essentially as hard spheres moving in a constant potential. We expect that between these two limiting cases, the correlations between nearest neighbors (and thus the free energy) should also be well approximated. While this method can not include the fluid phase, we

are really interested in the stability of the A15 lattice so that the only relevant aspect of the fluid-solid transition is melting. Instead of going into the details of the fluid HCSS phase and analyzing the transition with, for example, Ramakrishnan-Yussouff theory,<sup>52</sup> we can estimate the melting curve by extrapolating the zero-temperature FCC melting point, which is, as we will see, far enough from the other phase boundaries to suggest that the latter persist within the temperature range that we study.

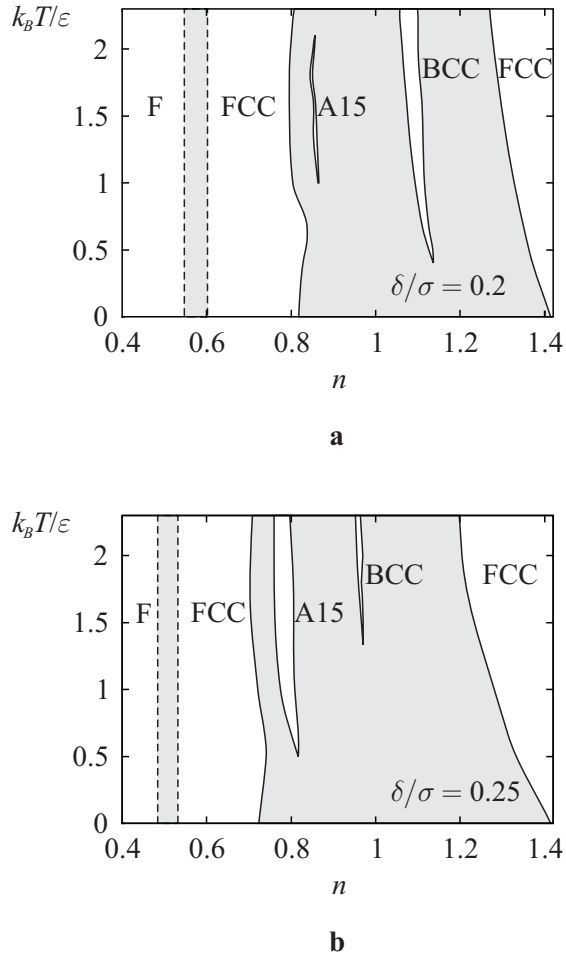


FIG. 11. Phase diagram of the hard-sphere-soft-shoulder potential for various shoulder widths: (a)  $\delta = 0.2$  and (b)  $\delta = 0.25$ . For these widths there is no expanded BCC lattice. The A15 lattice appears as one of the intermediate structures, interposed between the expanded and condensed FCC structures. The A15 islands of stability are elongated along the temperature axis, indicating that this structure should be sought after by varying the density rather than temperature. Note that the single-phase regions are small compared to coexistence regions. The dashed lines indicate the zero-temperature expanded FCC–fluid (F) coexistence.

Using this approach, we have analyzed the solid part of the phase diagram at low temperatures, focusing on the FCC, BCC, and A15 lattices. The coexistence be-

tween the phases was determined using the Maxwell double-tangent construction, and the results are shown in Figs. 11 and 12 for shoulder widths  $\delta/\sigma = 0.2, 0.25, 0.3$ , and  $0.35$ .

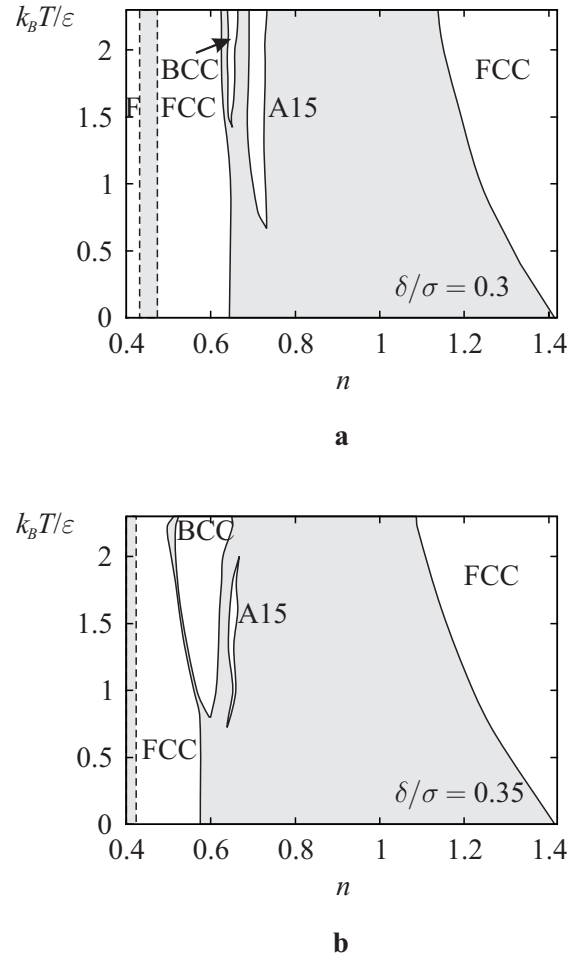


FIG. 12. Phase diagram of the hard-sphere-soft-shoulder potential for various shoulder widths: (a)  $\delta = 0.3$  and (b)  $\delta = 0.35$ . For these widths there is no condensed BCC lattice. As in the previous figure, the A15 lattice appears as one of the intermediate structures, interposed between the expanded and condensed FCC structures.

The main features of the phase diagram can be summarized as follows:

(i) We find that the A15 lattice can be a stable state of the HCSS system between the expanded and condensed FCC phase. As expected from the structure of the pair distribution function, this lattice is stable for shoulders neither too narrow (which would make the particles too similar to ordinary hard spheres) nor too broad (which would destroy the comparative advantage of the A15 lattice over the FCC and BCC lattices). The minimal and the maximal shoulder widths roughly correspond to  $\delta = 0.2$  and  $0.35$ , respectively. Note that these widths are consistent with the structural parameters of the den-

dimer compound where this lattice was observed experimentally, although the effective hard core of the micelles may not necessarily coincide with the benzyl inner segment of the dendrimers.

Temperature is also a crucial parameter of the stability of the A15 lattice and should not be too low nor too high. The A15 island in the phase diagram appears to be centered around  $k_B T/\epsilon \approx 1.4$  and its temperature range spans about  $2k_B T/\epsilon$  at most, the maximum being at  $\delta \approx 0.27$ . The A15 lattice is a delicate structure: for all  $\delta$  and  $T$ , the pure A15 structure occurs only within a rather narrow range of density centered at  $n \approx 0.85$  with width  $\Delta n \approx 0.05$ .

(ii) In the density-temperature plane, islands of stability of the intermediate-density solid phases (*i.e.*, expanded FCC, expanded BCC, A15, and condensed BCC lattice) are elongated along the temperature axis, implying that over broad ranges of temperature, the phase sequence does not change dramatically with density. This departs from the low-temperature extrapolations of the results of perturbative theory:<sup>48</sup> the stripe-like topology of the phase diagrams presented in Fig. 11 and Fig. 12 is free of critical and/or triple points as well as the corresponding isostructural transitions. This is most likely a consequence of the rather broad shoulder.

(iii) For shoulders as broad as necessary to stabilize the A15 lattice, the phase diagram is characterized by relatively small islands of stability of the intermediate phases: two-phase coexistence dominates the phase diagram. This feature appears to be specific to convex interparticle potentials, whereas in case of concave potentials the regions of coexistence are typically much narrower.<sup>53</sup>

While the stability of the A15 lattice is certainly not limited to HCSS potentials, our findings indicate that at least in some systems it could coexist with FCC, BCC, or perhaps another lattice over a rather wide density range. As far as the structural identification of the samples is concerned, this simple fact may have important consequences. In the case of phase coexistence, the interpretation of X-ray measurements is difficult. In practice, the space groups of the coexisting phases can only be determined unambiguously by varying the external parameters and moving from one island of stability across the coexistence region to the other island of stability. Given the stripe-like topology of the phase diagram, the parameter to be varied should be the density and not temperature. Even with this proviso, the identification can be difficult because of a considerable overlap between the diffraction peaks of the structures involved. For example, the difference between the patterns of A15 and BCC lattice is not very striking – the reflections being at  $\sqrt{2}, \sqrt{4}, \sqrt{5}, \sqrt{6}, \dots$  and at  $\sqrt{2}, \sqrt{4}, \sqrt{6}, \dots$  for the A15 and BCC lattices, respectively<sup>54</sup> – and could be masked by the form factor of the particles, which usually falls off quite rapidly with the wavevector.<sup>36</sup> These shortcomings could be overcome by complementing the X-ray studies by calorimetric measurements.

Last but not least, we note that the relative rarity of

the A15 lattice in real colloidal crystals may be caused by other, non-equilibrium mechanisms that can slow down the formation of a pure A15 colloidal crystal. For example, it is conceivable that the relatively simpler BCC lattice is kinetically favored over the A15 lattice in experiments which evaporate solvent to form crystallites. Given that the free energies of the different lattices are typically rather small, the equilibration can take very long and the actual ground state may be hard to observe.

Nevertheless, along with recent experimental<sup>14</sup> as well as theoretical studies<sup>10</sup> our preliminary results point to the necessity of extending the phase diagram of soft spherical particles by the A15 lattice and possibly other non-close-packed lattices. At the same time, the more intricate phase diagram may be more difficult to determine and understand.

#### IV. CONCLUSIONS

In this study, we have extended the geometrical interpretation of the free energy of weakly interacting classical particles, and we have complemented the well-known close-packing rule with a minimal-area rule. The incompatibility of the two principles leads to frustration which gives rise to range of possible equilibrium structures, depending on the relative weight of the two terms. Our proposed scheme is a computationally simple, zeroth-order description of soft-sphere crystals which is more transparent than detailed numerical models, most notably molecular modeling.

As such, our theory provides a robust insight into the self-organization of such objects, which should be useful for the engineering of colloidal crystals. The relevance of these universal guidelines is as broad as the use of colloids themselves, ranging from photonic bandgap crystals<sup>55,56</sup> to micro- or mesoporous materials used for chemical microreactors and molecular sieves.<sup>57,58</sup> To meet the demands of a particular application, these designer materials must be characterized by a given lattice constant, symmetry, and mechanical properties, and, in the case of porous structures, void size and connectivity. All these parameters can be controlled by tuning the structure and size of the (template) colloidal particles and the interaction between them, and our model establishes a semi-quantitative relationship between particle geometry and bulk material properties.

We envision this work to be extended in several directions. One problem to be addressed is to locate the A15 lattice within the phase diagram using Monte Carlo analysis, starting with a square-shoulder potential but also employing less generic short-range potentials. In addition, we will further explore the analogy between colloidal crystals and soap froths in view of the geometrical approach that we have adopted here. Another interesting aspect of future work could be to use the model to derive some of the mechanical properties of colloidal crys-

tals, such as the shear and Young moduli. One could also study the stability of non-cubic lattices, which have been mostly neglected so far, in an attempt to understand non-spherical colloidal particles. Work along these lines should lead to easily verifiable predictions and a deeper insight into the physics of colloids.

## ACKNOWLEDGMENTS

We gratefully acknowledge stimulating conversations with M. Clerc-Imp eror, G.H. Fredrickson, W.M. Gelbart, P.A. Heiney, C.N. Likos, T.C. Lubensky, V. Percec, J.-F. Sadoc, and A.G. Yodh.

This work was supported in part by NSF Grants DMR97-32963, DMR00-79909 and INT99-10017, the Donors of the Petroleum Research Fund, administered by the American Chemical Society, and a gift from L.J. Bernstein. R.D.K. was also supported by the Alfred P. Sloan Foundation.

---

\* On leave from J. Stefan Institute, Slovenia.

<sup>1</sup> Yablonovitch, E. *Phys. Rev. Lett.* **1987**, *58*, 2059.

<sup>2</sup> John, S. *Phys. Rev. Lett.* **1987**, *58*, 2486.

<sup>3</sup> Russel, W.B.; Saville, D.A.; Schowalter, W.R. *Colloidal Dispersions*, Cambridge University Press: Cambridge, 1989.

<sup>4</sup> Hone, D.; Alexander, S.; Chaikin, P.M.; Pincus, P. *J. Chem. Phys.* **1983**, *79*, 1474.

<sup>5</sup> Kremer, K.; Robbins, M.O.; Grest, G.S. *Phys. Rev. Lett.* **1986**, *57*, 2694.

<sup>6</sup> Rosenberg, R.O.; Thirumalai, D. *Phys. Rev. A* **1987**, *36*, 5690.

<sup>7</sup> Rasc n, C.; Velasco, E.; Mederos, L.; Navascu es, G. *J. Chem. Phys.* **1997**, *106*, 6689.

<sup>8</sup> Bolhuis, P.; Frenkel, D. *J. Phys. C* **1997**, *9*, 381.

<sup>9</sup> Stell, G.; Hemmer, P.C. *J. Chem. Phys.* **1972**, *56*, 4274.

<sup>10</sup> Watzlawek, M.; Likos, C.N.; L wen, H. *Phys. Rev. Lett.* **1999**, *82*, 5289.

<sup>11</sup> Mau, S.-C.; Huse, D.A. *Phys. Rev. E* **1999**, *59*, 4396.

<sup>12</sup> Hales, T. C. *Notices Amer. Math. Soc.* **2000**, *47*, 440.

<sup>13</sup> Rivier, N. *Phil. Mag. Lett.* **1994**, *69*, 297.

<sup>14</sup> Balagurusamy, V. S. K.; Ungar, G.; Percec, V.; Johansson, G. *J. Am. Chem. Soc.* **1997**, *119*, 1539.

<sup>15</sup> Zihlerl, P.; Kamien, R.D.; *Phys. Rev. Lett.* **2000**, *85*, 3528.

<sup>16</sup> Chemical formula: methyl 3,4,5-tris-3',4',5'-[tris (*n* - dodecyloxy) benzyloxy]bezoic acid, *n* = 2, 3 or 4 denotes the generation of the dendrimer.

<sup>17</sup> Percec, V.; Ahn, C.-H.; Ungar, G.; Yeardley, D.J.P.; M ller, M.; Sheiko, S.S. *Nature* **1998**, *391*, 161.

<sup>18</sup> Hudson, S.D.; Jung, H.-T.; Kewsuwan, P.; Percec, V.; Cho, W.-D. *Liq. Cryst.* **1999**, *26*, 1493.

<sup>19</sup> Thomson, W. *Phil. Mag.* **1887**, *24*, 503.

<sup>20</sup> Klarreich, E. *American Scientist* **2000**, *88*, 152.

<sup>21</sup> Taylor, J.E. *Ann. Math.* **1976**, *103*, 489.

<sup>22</sup> T.C. Hales, *Discrete Comput. Geom.* **25**, 1 (2001).

<sup>23</sup> Weaire, D.; Phelan, R. *Phil. Mag. Lett.* **1994**, *69*, 107.

<sup>24</sup> Kl eman, M.; Sadoc, J.-F. *J. Phys. (Paris) Lett.* **1979**, *40*, L569.

<sup>25</sup> Sadoc, J.-F.; Mosseri, R. *Geometrical Frustration*, Cambridge University Press: Cambridge, 1999.

<sup>26</sup> Weaire, D. Ed., *The Kelvin Problem: Foam Structures of Minimal Surface Area*, Taylor & Francis: London, 1997.

<sup>27</sup> Brakke, K. *Exp. Math.* **1992**, *1*, 141.

<sup>28</sup> Glazier J.A.; Weaire, D. *Phil. Mag. Lett.* **1994**, *70*, 351.

<sup>29</sup> Hill, T.L. *Statistical Mechanics*, McGraw-Hill: New York, 1956.

<sup>30</sup> Barker, J.A. *Lattice Theory of the Liquid State*, Pergamon: Oxford, 1963.

<sup>31</sup> Curtin W.A.; Runge, K. *Phys. Rev. A* **1987**, *35*, 4755.

<sup>32</sup> Kittel, C. *Introduction to Solid State Physics*, Wiley: New York, 1953.

<sup>33</sup> Crocker, J.C.; Grier, D.G. *Phys. Rev. Lett.* **1994**, *73*, 352.

<sup>34</sup> Milner, S.T.; Witten, T.A.; Cates, M.E. *Europhys. Lett.* **1988**, *5*, 413.

<sup>35</sup> Whetten, R.L.; Shafiqullin, M.N.; Khoury, J.T.; Schaaff, T.G.; Vezmar, I.; Alvarez, M.M.; Wilkinson, A. *Acc. Chem. Res.* **1999**, *32*, 397.

<sup>36</sup> McConnell, G.A.; Gast, A.P.; Huang, J.S.; Smith, S.D. *Phys. Rev. Lett.* **1993**, *71*, 2102.

<sup>37</sup> McConnell, G.A.; Gast, A.P. *Phys. Rev. E* **1996**, *54*, 5447.

<sup>38</sup> Charvolin, J.; Sadoc, J.-F. *J. Phys. (Paris)* **1988**, *49*, 521.

<sup>39</sup> Luzzati, V.; Delacroix, H.; Gulik, A. *J. Phys. II* **1996**, *6*, 405.

<sup>40</sup> Mariani, P.; Amaral, L.Q.; Saturni, L.; Delacroix, H. *J. Phys. II* **1994**, *4*, 1393.

<sup>41</sup> Clerc, M. *J. Phys. II* **1996**, *6*, 961.

<sup>42</sup> Matsen, M.W.; Bates, F.S. *J. Chem. Phys.* **1997**, *106*, 2436.

<sup>43</sup> Dotera, T. *Phys. Rev. Lett.* **1999**, *82*, 105.

<sup>44</sup> Hoover, W.G.; Ross, M.; Johnson, K.W.; Henderson, D.; Barker, J.A.; Brown, B.C. *J. Chem. Phys.* **1970**, *52*, 4931.

<sup>45</sup> Meijer, E.J.; El Azhar, F. *J. Chem. Phys.* **1997**, *106*, 4678.

<sup>46</sup> Lang, A.; Kahl, G.; Likos, C.N.; L wen, H.; Watzlawek, M. *J. Phys. C* **1999**, *11*, 10143.

<sup>47</sup> Velasco, E.; Mederos, L.; Navascu es, G.; Hemmer, P.C.; Stell, G. *Phys. Rev. Lett.* **2000**, *85*, 122.

<sup>48</sup> Velasco, E.; Mederos, L.; Navascu es, G. *Langmuir* **1998**, *14*, 5652.

<sup>49</sup> Hansen, J.P.; Macdonald, I.R. *Theory of Simple Liquids*, Academic Press: London, 1986.

<sup>50</sup> Technically, this was done by storing the accepted moves of the central particle and then assigning randomly selected accepted moves to its neighbors. The array of accepted moves was big enough so that the free energy did not depend on its size, and was updated continuously. After equilibration, this led to identical probability distributions at all equivalent positions.

<sup>51</sup> Kirkwood, J.G. *J. Chem. Phys.* **1950**, *18*, 380.

<sup>52</sup> Ramakrishnan, T.V.; Yussouff, M. *Phys. Rev. B* **1979**, *19*, 2775.

<sup>53</sup> Lang, A.; Likos, C.N.; Watzlawek, M.; L wen, H. *J. Phys. C* **2000**, *12*, 5087.

<sup>54</sup> T. Hahn, Ed., *International Tables for Crystallography*, D.

Reidel Publishing Company: Dordrecht, 1983.

- <sup>55</sup> Tarhan, İ.İ.; Watson, G.H. *Phys. Rev. Lett.* **1996**, *76*, 315.
- <sup>56</sup> Busch, K.; John, S. *Phys. Rev. E* **1998**, *58*, 3896.
- <sup>57</sup> Jenekhe, S.A; Chen, X.L. *Science* **1999**, *283*, 372.
- <sup>58</sup> Sakamoto, Y.; Kaneda, M.; Terasaki, O.; Zhao, D.Y.; Kim, J.M.; Stucky, G.; Shin, H.J.; Ryoo, R. *Nature* **2000**, *408*, 449.